JOINT INSTITUTE FOR AERONAUTICS AND ACOUSTICS

National Aeronautics and Space Administration
Ames Research Center

JIAA TR - 107

Stanford University

Sensitivity of the Structure of Untripped Mixing Layers To Small Changes In Initial Conditions

By

M. W. Plesniak, J. H. Bell and R. D. Mehta

Stanford University
Department of Aeronautics and Astronautics
Stanford, CA 94305

August 1992

Abstract

An experimental study has been conducted concerning the influence of small changes in initial conditions on the near- and far-field evolution of the three-dimensional structure of a plane mixing layer. A two-stream mixing layer with a velocity ratio of 0.6 was generated with the initial boundary layers on the splitter plate laminar and nominally two-dimensional. The initial conditions were changed slightly by interchanging the high- and low-speed sides of the wind tunnel, while maintaining the same velocities, and hence velocity ratio. This resulted in small changes in the initial boundary layer properties and the perturbations present in the boundary layers were interchanged between the high- and low-speed sides for the two cases. The results indicate that, even with this relatively minor change in initial conditions, the near-field regions of the two cases differ significantly. The peak Reynolds stress levels in the near-field differ by up to 100% and this is attributed to a difference in the location of the initial spanwise vortex roll-up. In addition, the positions and shapes of the *individual* streamwise vortical structures differ for the two cases, although the overall qualitative description of these structures is comparable. The subsequent reorganization and decay of the streamwise vortical structures is very similar for the two cases. As a result, in the far-field, both mixing layers achieve similar structure, yielding comparable growth rates, Reynolds stress distributions and spectral content.

List of Symbols

C_f:	Splitter plate skin friction coefficient
E_{uu}:	Power spectral density (u-component)
H:	Boundary layer shape factor
q_0:	Surface dynamic pressure in boundary layer
r:	U_2/U_1, Mixing layer velocity ratio
Re:	Reynolds number
s:	Mean streamwise vortex spacing
U, V, W:	Mean velocity in the X,Y,Z directions, respectively
U_e:	Local free-stream velocity in the wind tunnel
U_0:	$(U_1 - U_2)$, Velocity difference across mixing layer
u', v', w':	Fluctuating velocity components in the X,Y,Z directions, respectively
u, v, w:	Instantaneous velocity in the X,Y,Z directions, respectively, e.g. u = U + u'
X, Y, Z :	Cartesian coordinates for streamwise, normal, and spanwise directions, respectively
Γ:	Circulation of streamwise vortices
δ:	Mixing layer thickness (based on error function fit)
δ_{99}:	Boundary layer thickness
θ:	Boundary layer momentum thickness
λ:	$(U_1 - U_2)/(U_1 + U_2)$, Velocity ratio parameter
σ^2:	Variance
Ω_x:	Streamwise component of mean vorticity
$\overline{\quad}$:	(overbar) Time-averaged quantity
$()_{max}$:	Maximum value at given X-station (spanwise averaged)
$()_1$:	Value for high-speed side
$()_2$:	Value for low-speed side

1 Introduction

Since the 1940's, the plane turbulent mixing layer has been the object of extensive experimental and computational investigation. Its relatively simple mathematical description and self-similar solution make the mixing layer a desirable free-shear flow for fundamental studies. In addition, the mixing layer can be used as a building block to model more complex flows encountered in nature. Free-shear flows are prevalent in aerodynamics and combustion applications. In many of these applications, control of the structure and turbulence in the mixing layer can lead to enhanced mixing for improved performance in combustion, as well as lower NO_x emissions. Aerodynamic noise can also be reduced or modified through control of the shear layer. Thus, a great deal of effort has been directed toward understanding the generation and transport of turbulence in the mixing layer. However, these phenomena are not yet fully understood because this simple shear flow is generally found to be very sensitive to initial and boundary conditions (Rodi 1975, Ho and Huerre 1984).

Experimental studies conducted in the 1970's began to show that the near-field development of plane mixing layers was largely influenced by the formation and interaction of large-scale spanwise vortices within the layer (Brown and Roshko 1974). Further research indicated that the formation of the spanwise vortical structures was primarily caused by the inviscid Kelvin-Helmholtz instability operating on the velocity distribution across the mixing layer. Once these structures are formed, the layer grows linearly through the random amalgamation or pairing of adjacent spanwise vortices. In addition to the spanwise structures, some of the earlier (time-averaged) plan-view photographs of plane mixing layers also indicated the presence of distinct streamwise streaks which at the time were conjectured to signify an additional, streamwise oriented, vortical structure (Brown and Roshko 1974, Breidenthal 1981). The conjecture was later confirmed when cross-sectional views of the mixing layer were obtained over a wide range of Reynolds numbers (Bernal and Roshko 1986, Jimenez *et al.* 1985). These results clearly showed pairs of counter-rotating streamwise vortices riding within the spanwise structures.

The origin and development of the streamwise vorticity in the near-field region of a mixing layer was investigated qualitatively in several low Reynolds number ($Re_\delta \sim 10^3$) water channel experiments by Lasheras *et al* (1986). They suggested that the streamwise vortices were a result of "an unstable response of the layer to three-dimensional perturbations in the upstream conditions". This hypothesis was later confirmed by introducing small periodic perturbations along the splitter plate span to trigger the formation of the vortices (Lasheras and Choi 1988). It was found that streamwise structures, of scale somewhat smaller than the spanwise ones, first appeared in the braids (region connecting adjacent spanwise structures), before propagating into the spanwise vortex cores. These streamwise vortices were stretched and compressed by the strain field due to the spanwise vortices, but did not appear to affect the development of the spanwise structures significantly.

The role of these streamwise structures in a mixing layer at higher Reynolds number ($Re_\delta \sim 2.9 \times 10^4$) was recently investigated quantitatively by Bell and Mehta (1992). A plane, two-stream mixing layer was generated, with a fixed velocity ratio of 0.6 and laminar initial boundary layers which were nominally two-dimensional. Measurements of

the mean streamwise vorticity indicated that small disturbances (naturally present) in the flow were initially amplified just downstream of the first spanwise roll-up, leading to the formation of streamwise vortices, in agreement with the observations of Lasheras *et al* (1986). The streamwise vortices, with average circulation equivalent to about 10% of the initial spanwise circulation, first appeared in clusters containing vortices of both signs, but re-organized further downstream to form counter-rotating pairs. This vortex structure was found to grow in size, scaling approximately with the mixing layer vorticity thickness, and weaken, the maximum mean vorticity diffusing as approximately $1/X^{1.5}$. The mean streamwise vorticity was found to be strongly correlated in position, strength and scale with the secondary shear stress ($\overline{u'w'}$). The $\overline{u'w'}$ data suggested that the streamwise structures persisted through to the far-field region, although they were weak enough by this point that the mixing layer may be considered to be nominally two-dimensional.

Mixing layers are known to be very sensitive to initial conditions, and so one question which naturally arose in the above study was to what extent the details of the observed three-dimensionality were facility dependent, i.e. would the nature of the three-dimensionality be the same in *all* wind tunnels? Hence, the main objective of the present study was to establish the sensitivity of the three-dimensionality to small changes in initial conditions. In particular, qualitative and quantitative changes in the streamwise vorticity, and its effects on the mixing layer mean and turbulence properties, were to be determined in the near- and far-field regions through direct measurements. The slight change in initial conditions was achieved by simply swapping the high- and low-speed sides in the *same* mixing layer wind tunnel, while maintaining the same velocity ratio.

2 Experimental Apparatus and Techniques

The experiments were conducted in the *Mixing Layer Wind Tunnel*, consisting of two separate legs which are driven independently by centrifugal blowers connected to variable speed motors (Fig. 1). The "large" blower/motor combination has about three times the capacity compared to the "small" one. Two air streams merge at the sharp trailing edge of a slowly tapering splitter plate; the included angle at the splitter plate edge, which extends 15 cm into the test section, is about 1°. The test section is 36 cm in the cross-stream direction, 91 cm in the spanwise direction and 366 cm in length. One side-wall is adjustable, for streamwise pressure gradient control, and slotted, for probe access. In both cases described here, the flexible wall was adjusted to give a nominally zero streamwise pressure gradient.

For the present experiments, the high- and low-speed sides of the mixing layer were interchanged by adjusting the blower speeds appropriately. In the "base" case, the leg driven by the larger (15,000 CFM) blower was operated to provide a free-stream velocity of 15 m/s whereas the other leg was run at 9 m/s. In the other case, designated as the "reversed" case, the high- and low-speed sides were interchanged. Both cases were run at the same relative velocities, thus giving a fixed velocity ratio, $r = 0.6$ ($\lambda = 0.25$). The free-stream velocities were held constant to within 1% during a typical run lasting two hours. The measured streamwise turbulence level (u'/U_e) was approximately 0.15% and the transverse levels (v'/U_e and w'/U_e) were approximately 0.05%. The mean core-flow was found to be uniform to within 0.5% and cross-flow angles were less than 0.25° (Bell and

Mehta 1989b). The boundary layers on the splitter plate were laminar at these running conditions with the measured properties tabulated in Table 1. The tabulated values are averaged over profiles measured at five different spanwise locations. The spanwise variation of the tabulated properties was on the order of 2%, indicating the absence of any strong three-dimensional disturbances existing in the boundary layers. For a given velocity, the boundary layer properties agree reasonably well between the two sides of the splitter plate.

Table 1. Initial Boundary Layer Properties

Condition	U_e (m/s)	δ_{99} (cm)	θ (cm)	Re_θ	H
High-Speed Side, Base Case	15.0	0.40	0.053	525	2.52
Low-Speed Side, Base Case	9.0	0.44	0.061	362	2.24
High-Speed Side, Reversed Case	15.0	0.39	0.054	532	2.29
Low-Speed Side, Reversed Case	9.0	0.44	0.055	322	2.61

Measurements were made using a cross-wire probe mounted on a 3-D traverse and linked to a fully automated data acquisition and reduction system controlled by a MicroVax II computer. The cross-wire probe consisted of 5 μm tungsten sensing elements approximately 1 mm long and separated by about 1 mm. The probe was calibrated statically in the potential core of the flow assuming a 'cosine-law' response to yaw, with the effective angle determined by calibration. The analog signals were filtered (low pass at 30 Khz), DC offset, and amplified ($\times$ 10) before being fed into a computer interface. The interface contained a fast sample-and-hold A/D converter with 12 bit resolution and a multiplexer for connection to the computer (Bell and Mehta 1989a). Individual statistics were averaged over 5000 samples obtained at a rate of 400 samples per second.

Data were obtained in several $Y - Z$ planes with the probe oriented in the uv- and uw-planes. The data consisted of all three components of mean velocity, five independent components of the Reynolds stress tensor and selected higher-order products. Measurements were made at six (reversed case) to nine (base case) streamwise stations within the test section between $X = 8$ to 250 cm. Typically, 1200-2000 points were measured on a rectangular cross-plane grid at a given streamwise station. The grid spacing (same in Y and Z directions) ranged from 0.1 to 0.25 cm at the most upstream stations; it was increased to 0.5 cm at the intermediate stations and to 1 cm at the furthest downstream stations. The measurements of U, W and $\overline{u'w'}$ were corrected for mean streamwise velocity gradient ($\partial U/\partial Y$) effects (Bell and Mehta 1989a). The streamwise component of mean vorticity (Ω_x) was computed from the V and W velocity measurements using a central difference approximation. The overall circulation (Γ) was determined from a surface integral of the streamwise vorticity field over the cross-plane, with vorticity levels less than 20% of the maximum value being set to zero in order to provide immunity from "noise".

3 Results and Discussion

In order to illustrate the similarities and differences between the base and reversed cases, detailed comparisons at selected streamwise locations are presented below covering both the near- and far-field development regions. Recall that the two cases are nominally the same, i.e., the free-stream velocities and velocity ratio are identical. The only difference is that the high- and low-speed sides are interchanged in the *same facility*.

Figures 2a-c present contours of the mean streamwise velocity for the two cases at three measurement stations. At the first location (X = 8 cm), the velocity contours are somewhat distorted in both cases, but in an irregular fashion. This distortion is caused by the presence of streamwise vortices in the mixing layer. Note that the spatial distribution of the distortions is slightly different for the base and reversed cases, suggesting that the exact nature of the initial streamwise vorticity may not be the same. Further downstream, the distortions become more regular and extend all the way across the mixing layer. By X = 78 cm, a distinct wavelength of about 5 cm is observed in the spanwise distortions for both cases. Again, the distributions are slightly different in detail — note, for example, that the distortions are more regular on the positive-Z side for the base case. Further downstream, the distortions appear to decrease in amplitude and increase in wavelength. Figure 2c illustrates mean streamwise velocity contours for the two cases at the far downstream measuring station at X = 189 cm. In both cases, the contour lines are almost straight and quasi-parallel, as would be expected in a two-dimensional flow. Thus, in the mean sense, both flows eventually seem to develop into a quasi-two-dimensional state.

Streamwise evolution plots of the mixing layer thickness and peak Reynolds stresses are presented in Figs. 3-5 for the base and reversed cases. All the results are based on spanwise averaged quantities, i.e. the measurements, obtained on a cross-plane grid, are divided into profiles through the mixing layer and the properties computed for each profile, before being averaged with those obtained at other spanwise positions. In effect, the properties are averaged over 20 to 90 spanwise profiles, depending on the streamwise location. Spanwise averaging is necessary to obtain an accurate representation of the behavior of the mixing layer due to the large spanwise variations experienced in the near-field. The differences between spanwise-averaged mixing layer properties and those obtained from a single profile along the tunnel centerline (as has been the common practice), are demonstrated and discussed by Bell *et al.* (1992).

Figure 3 presents the streamwise growth of the mixing layer thickness (based on an error function fit to the mean streamwise velocity data) for the base and reversed cases. The mixing layer thickness and growth rates are quite close for the two cases — note that the growth is relatively slow between the first two stations. In the downstream region, both mixing layers exhibit linear growth with similar growth rates. Based on a linear least squares fit to the data downstream of X = 78 cm, the growth rate ($d\delta/dx$) for both cases is 0.023. As has been shown in previous studies (Mehta and Westphal 1986), a linear growth rate is not a very sensitive indicator that the asymptotic state of a mixing layer has been achieved; a better indicator for this is the behavior of the Reynolds stresses.

The streamwise evolution of the peak Reynolds normal stress components ($\overline{u'^2}$, $\overline{v'^2}$, and $\overline{w'^2}$) is shown in Fig. 4. Initially, in the near-field region, large overshoots caused by the transition process are apparent in both data sets. However, there are significant

differences in the maxima of the normal stresses, especially in $\overline{u'^2}$ and $\overline{v'^2}$. At $X = 8$ cm, the normal stresses are 50 to 100% higher in the reversed case compared to the base case. The relatively high differences in $\overline{u'^2}$ and $\overline{v'^2}$ suggest that the details of the initial spanwise vortex roll-up may be responsible for the observed effects. Note that the levels of $\overline{w'^2}$, which is not as strongly affected by the initial spanwise vortex roll-up, are much closer for the two cases. At $X = 17$ cm, the reversed case normal stress maxima are still 40% higher than in the base case. However, downstream of $X \sim 100$ cm, comparable asymptotic values are attained in both cases for each of the three normal stresses. In this region the asymptotic levels for all three normal stresses agree to within about 10%. Plots of these stresses in similarity coordinates (not shown here for reasons of brevity) also show that the profiles collapse adequately in this region and are comparable between the two cases.

Figure 5 illustrates the streamwise evolution of the (positive) primary Reynolds shear stress ($\overline{u'v'}$) maxima in the two cases. The peak shear stress levels in the development region are somewhat higher for the base case, but the eventual asymptotic levels of the peak shear stress are approaching the same limit ($\overline{u'v'}_{max}/{U_0}^2 \sim 0.011$) which agrees well with the value given by Townsend's (1976) classical analysis for a purely two-dimensional mixing layer. The peak shear stress for the reversed case also appears to achieve the asymptotic level in a shorter streamwise distance.

In order to further investigate the turbulence structure for the two cases, the velocity spectra were measured at several streamwise locations. Since the spectra for the three velocity components show similar trends, only the u-component spectra are presented here. Figures 6a and b show the measured spectra for the near- and far-field regions, respectively. The spectra at $X = 8$ cm show that the distributions of energy for both cases are qualitatively similar, with a fundamental peak at $f \sim 600$-650 Hz due to the primary spanwise vortex formation. The vortex formation frequency for the reversed case appears to be somewhat lower (by about 8%) which is consistent with the slightly higher boundary layer momentum thickness on the high-speed side (θ_1) for this case (Ho and Huerre 1984). In the base case, streamwise spectral measurements showed that the first vortex roll-up occured at $X \sim 5$ cm. Since θ_1 is slightly higher for the reversed case, the first spanwise vortex roll-up should occur further downstream compared to the base case (Ho and Huerre 1984). Thus, it is possible that the first roll-up occurs closer to the first measurement station at $X = 8$ cm in the reversed case, resulting in higher stresses being measured. This explains some, but not all, of the observed differences in the near-field stress levels between the two cases. The fact that the reversed case has more energy in the fundamental peak supports the notion that the higher strength of the spanwise vortex roll-up may also be responsible for the higher stress levels in this case. These differences obviously do not persist into the far-field region since the spectral results at $X = 189$ cm clearly show that the turbulence structure for both cases is identical.

Contours of $\overline{u'v'}$ are presented in Figs. 7a-c for both cases at three streamwise locations. At the first measurement station ($X = 8$ cm), negative $\overline{u'v'}$ predominates in both cases. The negative shear stress is associated with the passage of spanwise vortices which do not undergo pairing in this region (Oster and Wygnanski 1982). This effect of the individual spanwise vortices passing by is also reflected in the $\overline{u'^2}$ profiles (not presented

here) which exhibit a double-peaked distribution (Bell and Mehta 1990). The lack of vortex pairing is the reason why the mixing layer grows relatively slowly between the first two stations. At the first station, the (spanwise-averaged) peak negative $\overline{u'v'}$ is -.014 for the base case, and -.038 for the reversed case. This is a further indication that the first spanwise vortex roll-up occurs closer to this measurement station in the reversed case. Also, the distribution of negative $\overline{u'v'}$ appears more two-dimensional for the reversed case, as might be expected immediately downstream of the vortex roll-up.

At X = 78 cm, the contours for both cases exhibit a quasi-periodic distortion, similar to that in the mean velocity contours. In addition, there are local peaks close to the mixing layer centerline, the magnitude of which is comparable for the two cases. In contrast to the distribution of $\overline{u'v'}$ at the upstream stations, Fig. 7c shows a quasi-two-dimensional distribution of $\overline{u'v'}$ for both cases at X = 189 cm. Spanwise variations of only 7% are measured at this position in both cases, although the averaged peak levels for the base case are slightly higher (by about 9%). Variations of this order are within the measurement accuracy of the hot-wire anemometry system for this quantity. Contours of the Reynolds normal stresses ($\overline{u'^2}$, $\overline{v'^2}$, and $\overline{w'^2}$) are not shown, but in general, exhibit similar trends as the primary shear stress. Their distributions are also different for the two cases at the upstream measurement stations, but tend toward quasi-two-dimensionality in the far-field region.

Bell and Mehta (1992) showed that the spanwise variations in the mean velocity and Reynolds stress distributions in the developing region of the mixing layer were governed by the position and strength of the secondary streamwise vortices. Figures 8a-d present contours of mean streamwise vorticity, Ω_x, at four measurement stations for the two cases. At X = 8 cm, it may be observed that the spanwise distribution of Ω_x is qualitatively similar for the two cases, in that the vortices appear in clusters of three, although the positions and shapes of the clusters are not exactly the same. The absolute peak vorticity levels, however, are not too dissimilar. By the second station (X = 17 cm), the clusters in both cases have started to "unravel" and the vortices are rounder in shape and contain lower peak vorticity levels. The clusters are still clearly identifiable and now typically contain about four vortices in both cases. By the X = 78 cm station, an orderly array of streamwise vortices of alternating sign is observed in ***both*** cases with approximately eleven vortices in the ±15 cm spanwise range. It is understandable that the streamwise vortices would continue to re-align until an "equilibrium", or most stable, configuration is achieved whereby the vortices are positioned in counter-rotating pairs (of comparable strength) across the entire mixing layer span. While the structures in the two cases are the same qualitatively, there are differences in the details of their distribution across the span. The peak vorticity levels in both cases have diminished compared to the upstream station. Figure 8d shows an apparently random distribution of very weak streamwise vorticity in both cases at X = 189 cm. At this position, the vorticity levels are so low that they are embedded within the "noise" level of the measurements. The contours at the top and bottom of the plot are remnants of the differentiation technique at the edges of the measurement domain and are considered noise as well. The absence of organized strong streamwise vortices at this streamwise location is consistent with the observed quasi-two-dimensionality of the mean streamwise velocity and Reynolds stress contours.

In both cases, the qualitative behavior of the streamwise vorticity is the same — it appears in clusters, re-organizes into counter-rotating pairs and decays and grows in scale with downstream distance, such that by the last measurement station the mixing layer is nominally two-dimensional. However, some of the differences noted in the streamwise vortex distributions in the very near-field warrant further examination.

Spanwise measurements of the mean streamwise velocity distributions in the initial boundary layers and immediately downstream of the splitter plate edge at $X \leq 4$ cm (not presented here) showed no systematic large amplitude variations, thus confirming that the initial shear layer has a nominally two-dimensional structure. The first signs of spanwise variations are observed downstream of the point where the initial spanwise roll-up occurs ($X \sim 5$ cm). This strongly suggests that the formation of the streamwise structures occurs in the braid region, a region of large positive strain. The most likely mechanism for this is through the stretching of weak incoming streamwise vorticity. Initially, the amplification must be expected to occur at locations determined by the strength and position of the incoming spatial perturbation. Although the mean streamwise velocity measurements indicate that the initial boundary layers are nominally two-dimensional, this does not preclude the presence of weak streamwise vorticity which is usually determined by the geometric details of the last screen in the settling chamber (Mehta and Hoffmann 1987). This vorticity is normally too weak to measure directly, but it may be adequately characterized by measuring the spanwise distribution of the skin friction coefficient (C_f).

Figures 9a and b show the spanwise distribution of the surface dynamic pressure (q_0) measured in the boundary layers on the splitter plate for the two cases. The spanwise variation of q_0 reflects the variation of C_f^2 in laminar boundary layers. Note that for both cases, the boundary layer on the side driven by the smaller blower exhibits a nearly flat distribution of q_0 across the span, while that on the large blower side exhibits a quasi-periodic variation in this quantity. In agreement with previous observations (Mehta and Hoffmann 1987), the distribution of q_0 in the present study is demonstrated to be essentially independent of Reynolds number, since it is basically preserved when the high- and low-speed sides are interchanged. Consequently, in the reversed case, the high-speed boundary layer contains the flat distribution of q_0 while the low-speed boundary layer has the periodic distribution. Examination of Fig. 9a reveals that, initially, Ω_x in both cases is clustered in groups, although the exact cluster positions are not the same. For the base case, about four clusters are observed, with their positions approximately consistent with the positions of the q_0 extrema on the large blower side, although the clusters on the positive-Z side are not as strong or as well defined as the others. Approximately four clusters are also observed in the reversed case (including half a cluster measured at $Z \sim$ -3 cm), but their positions do not seem to be strongly correlated with the q_0 extrema. In particular, the two strong clusters at $X \sim \pm$ 1 cm appear to be generated by the single peak in q_0 at $X \sim 0$. The main reason for this observed difference is not apparent, although it may be noted that for the base case the side with the higher q_0 variation is the high-speed side, whereas in the reversed case it becomes the low-speed side.

The development of some of the global streamwise vortex properties is presented in Figs. 10a-c. These properties were averaged over all vortices identified in the vorticity contour plots. The peak mean vorticity shown in Fig. 10a was evaluated by averaging the

maximum vorticity (absolute value) of all vortices identified at a given streamwise station. The peak mean vorticity levels for both cases are about the same and their decay rates are also similar; the decay approximately follows a $1/X^{1.5}$ relation. The overall streamwise vortex circulation for the two cases (Fig. 10b) also shows similar trends and the levels, by and large, are also comparable. The circulation remains approximately constant with downstream distance, with a temporary increase at $X \sim 40$-50 cm in both cases. The vortex spacing (Fig. 10c) is simply evaluated by dividing the measurement span by the number of identified vortices. Once again, the trends and spacing values are not too dissimilar for the two cases, especially considering the fewer number of data points in the reversed case. In addition, the overall rate of increase of the vortex spacing is also comparable such that the spacing scales with the mixing layer vorticity thickness. Note how the vortex spacing increases in the same region as the temporary increase in circulation ($X \sim 40$-50 cm). This implies that the increase in vortex spacing is probably caused by an amalgamation of the streamwise vortices. More detailed discussions of the behavior of these streamwise vortex properties are given in Bell and Mehta (1992).

It has been found that relatively small changes in initial conditions, while affecting the details of the near-field three-dimensional structure and Reynolds stress distributions, do not change the mixing layer global properties significantly. Once formed, the qualitative behavior of the streamwise vortices is also unaffected by the change in initial conditions. Furthermore, the streamwise development of the global streamwise vortex properties, such as the mean peak vorticity, circulation and spacing are comparable for the two cases. The far-field structure of the mixing layer in both cases is also very similar, in terms of thickness, growth rate, turbulence structure and peak stress levels.

4 Conclusions

An experimental study which shows the effects of relatively small changes in the initial conditions on the development of the three-dimensional structure of a plane mixing layer originating from laminar boundary layers has been completed. Two mixing layers (with the same velocity ratio) created by interchanging the high- and low-speed sides in the *same facility* were investigated.

It was shown that the near-field region of the mixing layer is extremely sensitive to initial conditions. Although the streamwise vortices first appeared in clusters of three in both cases, the exact shapes and positions of the clusters and peak amplitude distributions of the Reynolds stresses were quite different in the near-field region. The preferred spatial location of the clusters seems to be weakly related to extrema in the spanwise distribution of the boundary layer skin friction coefficient. Further downstream, the clusters re-align to form pairs of counter-rotating vortices in both cases. The presence of the (spatially stationary) streamwise vortices leads to significant spanwise distortions in the mean and turbulence properties of the mixing layer. The maximum vorticity diffuses rapidly with increasing downstream distance, while the vortices grow, scaling with the mixing layer vorticity thickness. As the streamwise vorticity decays (approximately as $1/X^{1.5}$) both mixing layers approach a quasi-two-dimensional state and are indistinguishable in terms of growth rate, Reynolds stress distributions and spectral content.

The present results indicate that small changes in initial conditions may affect the

Reynolds stress distributions in the near-field significantly. The most likely mechanism for this is through the effects of very small changes in initial boundary layer properties on the details of the spanwise vortex roll-up. This effect has important implications in terms of the approach of the mixing layer to self-similarity — for example, the streamwise development of the peak primary shear stress is quite different for the two cases. It is also worth noting that direct comparisons of the near-field development of mixing layers generated in different facilities may not be very useful because of this strong sensitivity to initial conditions. Despite these relatively large differences in the near-field, both mixing layers attain comparable turbulence structure and growth rates in the far-field. This is *not* always the case — for example, this same mixing layer with tripped initial boundary layers exhibits similar Reynolds stress comparisons, but its growth rate in the far-field region is about 25% lower (Bell and Mehta 1990).

The results clearly show that the streamwise vortical structures play a very important role in the development of mixing layers originating from laminar initial boundary layers and they must be included in all modeling of this important shear flow. Although some of the specific details of the secondary structure, such as the exact shape, position and strength, may be facility dependent, the indications are that a relatively strong structure, which produces significant three-dimensionality, should form in *all* mixing layers, regardless of the wind tunnel facility. After some initial readjustments, the structure should appear in the form of counter-rotating pairs of streamwise vortices which, in the mean, grow with the mixing layer and decay in strength. It is interesting to note that the overall global behavior of the streamwise vortex structure is quite similar between the two cases, despite the relatively large differences in the near-field Reynolds stress levels.

Acknowledgments

The authors wish to acknowledge the many helpful discussions with Professor James P. Johnston of Stanford University. This research was supported by The National Science Foundation Grant NSF-MSM-88-15670 and NASA Grant NCC-2-55 from the Fluid Mechanics Laboratory (FML), NASA Ames Research Center and conducted in the FML.

References

Bell, J.H.; Mehta, R.D. 1989a: Three-Dimensional Structure of Plane Mixing Layers. Report *JIAA TR-90*, Dept. of Aeronautics and Astronautics, Stanford University.

Bell, J.H.; Mehta, R.D. 1989b: Design and Calibration of the Mixing layer Wind Tunnel. Report *JIAA TR-84*, Dept. of Aeronautics and Astronautics, Stanford University.

Bell, J.H.; Mehta, R.D. 1990: Development of a Two-Stream Mixing Layer With Tripped and Untripped Boundary Layers. *AIAA Journal*, Vol. 28, No. 12, pp. 2034-2042.

Bell, J.H.; Plesniak, M.W.; Mehta, R.D. 1992: Spanwise Averaging of Plane Mixing Layer Properties. *AIAA Journal*, Vol. 30, No. 3, pp. 835-837.

Bell, J.H.; Mehta, R.D. 1992: Measurements of the Streamwise Vortical Structures in a Plane Mixing Layer. *Journal of Fluid Mechanics*, Vol. 239, pp. 213-248.

Brown, G.L.; Roshko, A. 1974: On Density Effects and Large Structure in Turbulent Mixing Layers. *Journal of Fluid Mechanics*, Vol. 64, pp. 775-816.

Bernal, L.P.; Roshko, A. 1986: "Streamwise Vortex Structure in Plane Mixing Layers. *Journal of Fluid Mechanics*, Vol. 170, pp. 499-525.

Breidenthal, R. 1981: Structure in Turbulent Mixing Layers and Wakes Using a Chemical Reaction. *Journal of Fluid Mechanics*, Vol. 109, pp. 1-24.

Ho, C.-M.; Huerre, P. 1984: Perturbed Free Shear Layers. *Annual Review of Fluid Mechanics*, Vol. 16, pp. 365-424.

Jimenez, J.; Cogollos, M.; Bernal, L.P. 1985: A Perspective View of the Plane Mixing Layer. *Journal of Fluid Mechanics*, Vol. 152, pp. 125-143.

Lasheras, J.C.; Cho, J.S.; Maxworthy, T. 1986: On the Origin and Evolution of Streamwise Vortical Structures in a Plane, Free Shear Layer. *Journal of Fluid Mechanics*, Vol. 172, pp. 231-258.

Lasheras, J.C.; Choi, H. 1988: Stability of a Plane Turbulent Shear Layer to Axial Perturbations. *Journal of Fluid Mechanics*, Vol. 189, pp. 53-86.

Mehta, R.D.; Westphal, R.V. 1986: Near-Field Turbulence Properties of Single- and Two-Stream Plane Mixing Layers. *Experiments in Fluids*, Vol. 4, pp. 257-266.

Mehta, R.D.; Hoffmann, P.H. 1987: Boundary Layer Two-Dimensionality in Wind Tunnels. *Experiments in Fluids*, Vol. 5, No. 5, pp. 358-360.

Oster, D.; Wygnanski, I.J. 1982: The Forced Mixing Layer between Parallel Streams. *Journal of Fluid Mechanics*, Vol. 123, pp. 91-130.

Rodi, W. 1975: A Review of Experimental Data of Uniform Density Free Turbulent Boundary Layers *Studies in Convection*, Vol. 1, ed. B. E. Launder, London: Academic Press, pp. 79-165.

Townsend, A.A. 1976: *Structure of Turbulent Shear Flow* (Cambridge University Press, Cambridge).

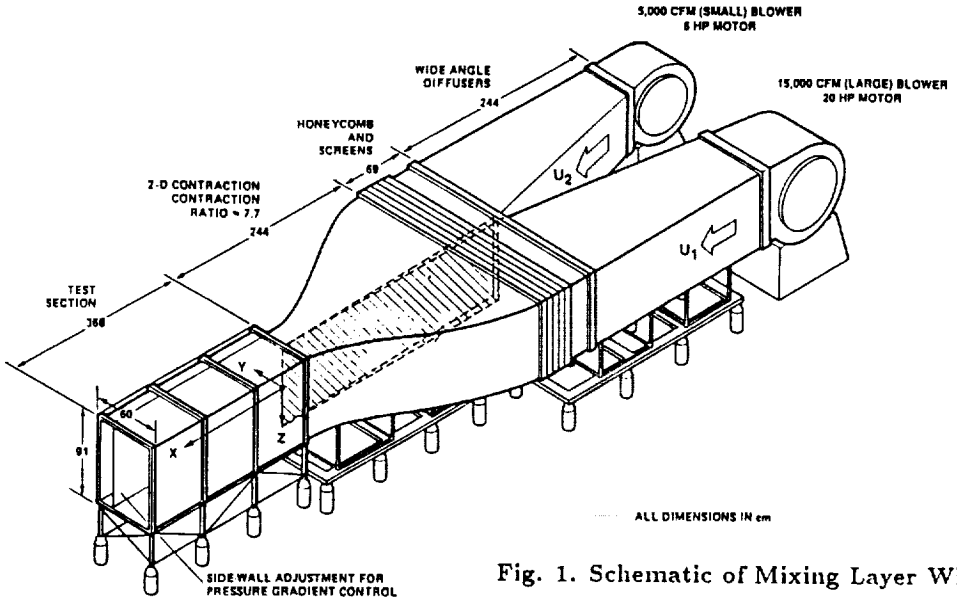

Fig. 1. Schematic of Mixing Layer Wind Tunnel.

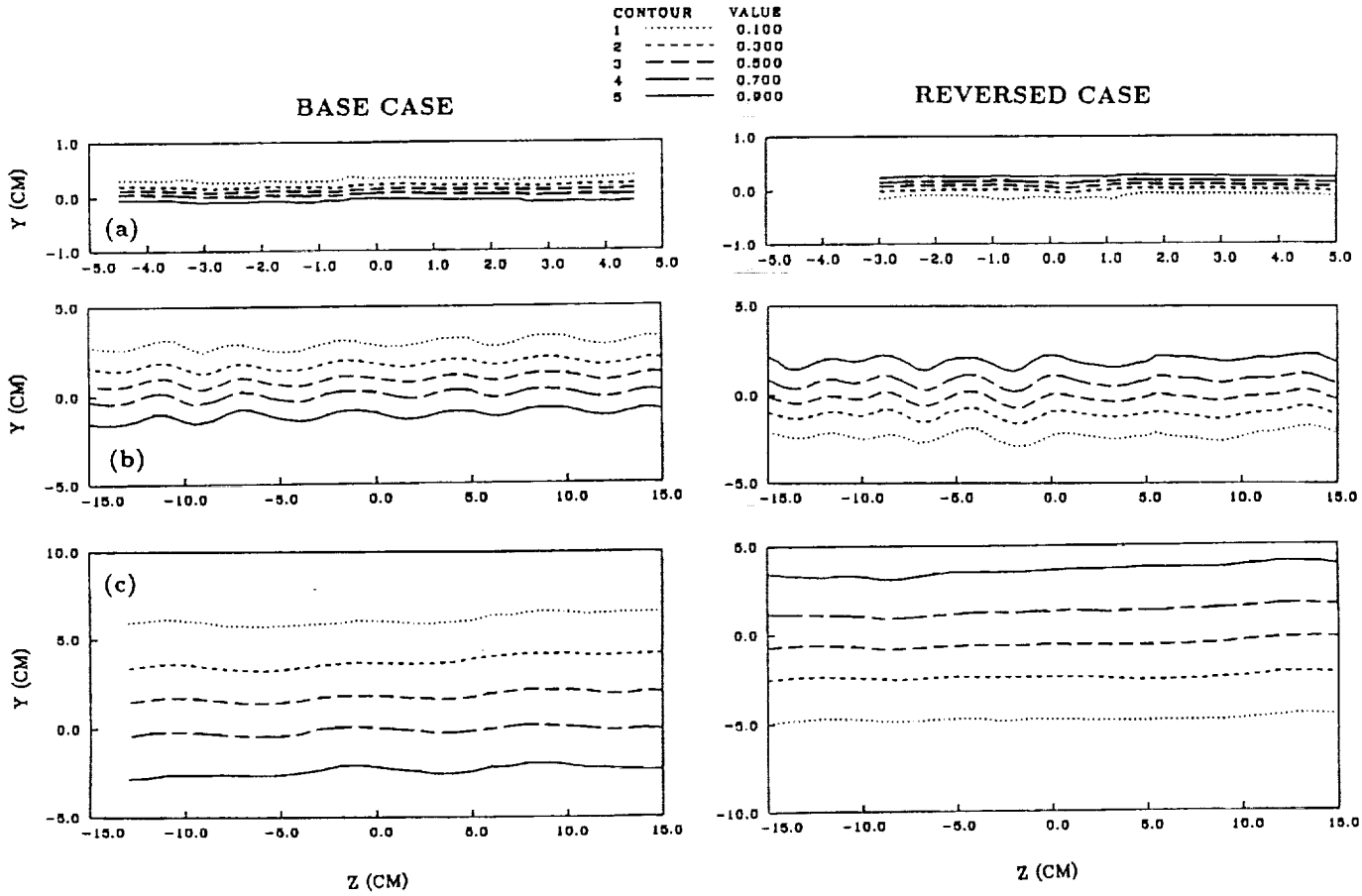

Fig. 2. Comparison of Mean Streamwise Velocity $[(U - U_2)/U_0]$ Contours for Base and Reversed Cases. (a) $X = 8$ cm, (b) $X = 77$ cm, (c) $X = 189$ cm.

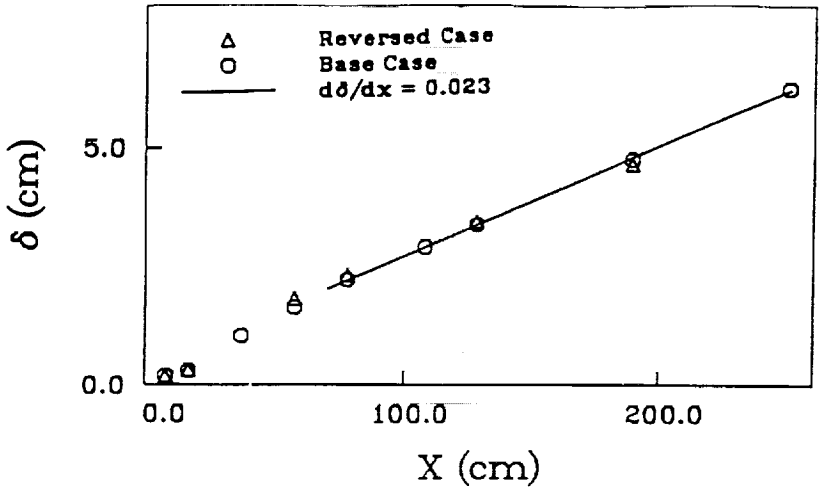

Fig. 3. Streamwise Development of the (spanwise averaged) Mixing Layer Thickness for Base and Reversed Cases.

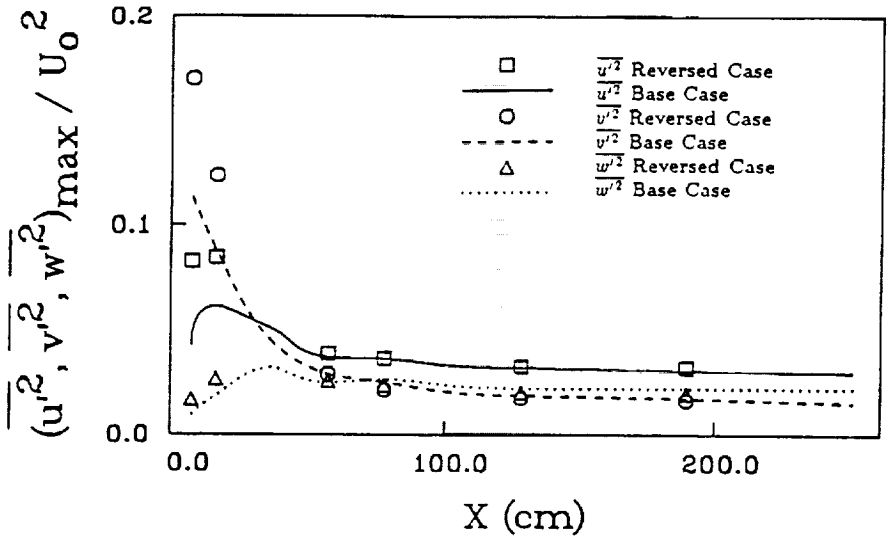

Fig. 4. Streamwise Development of the (spanwise averaged) Reynolds Normal Stresses for Base and Reversed Cases.

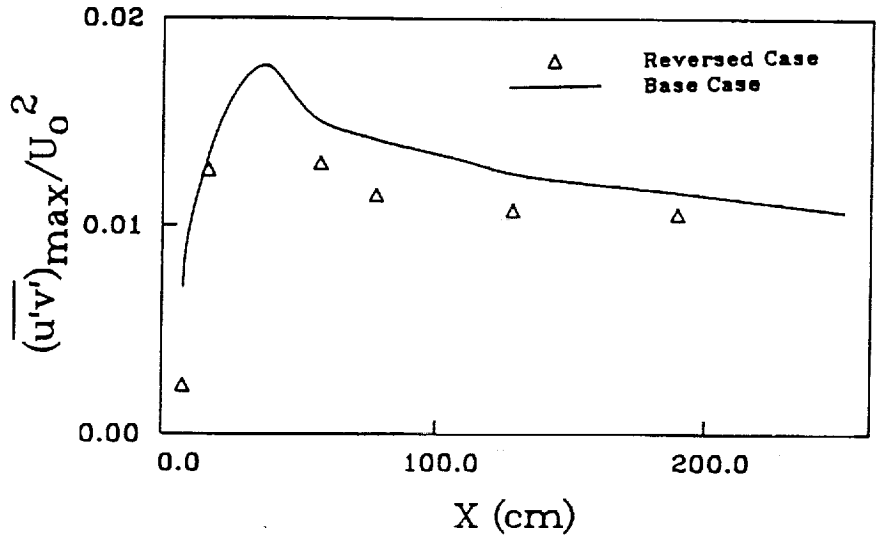

Fig. 5. Streamwise Development of the (spanwise averaged) Primary Reynolds Shear Stress for Base and Reversed Cases.

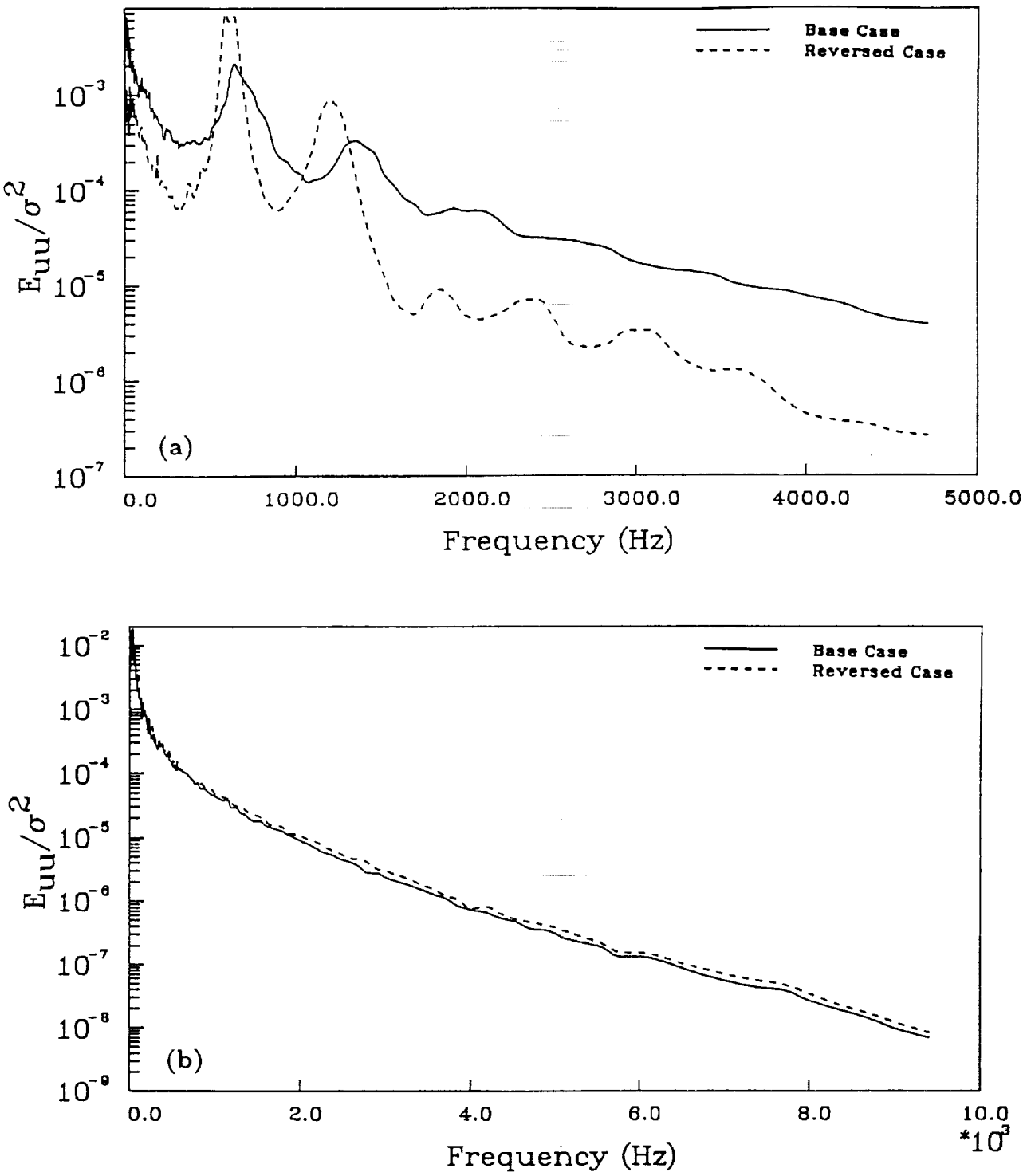

Fig. 6. u-Component Spectral Measurements for Base and Reversed Cases. (a) $X = 8$ cm, (b) $X = 189$ cm.

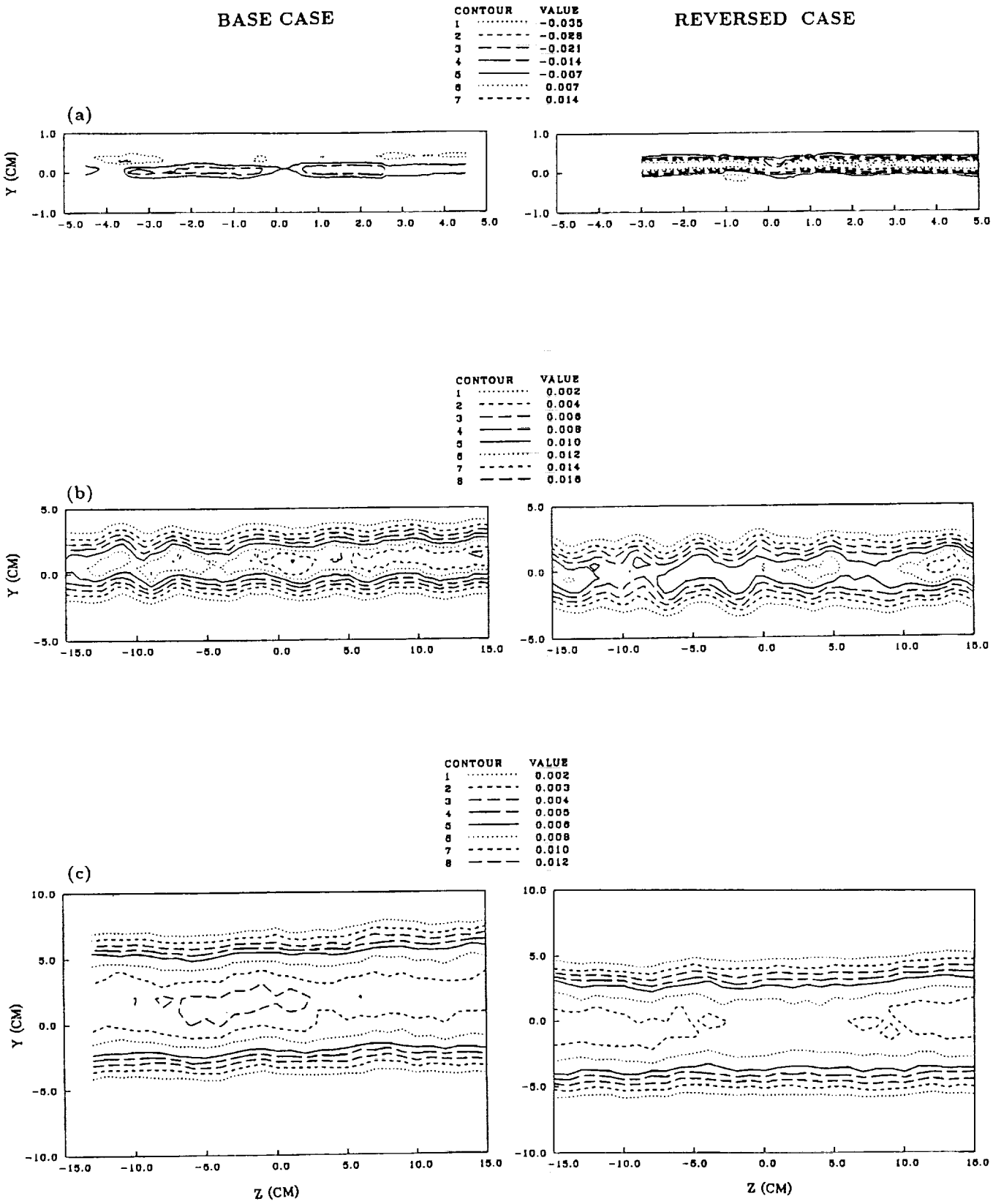

Fig. 7. Comparison of Primary Reynolds Shear Stress ($\overline{u'v'}/U_0^2$) Contours for Base and Reversed Cases. (a) $X = 8$ cm, (b) $X = 77$ cm, (c) $X = 189$ cm.

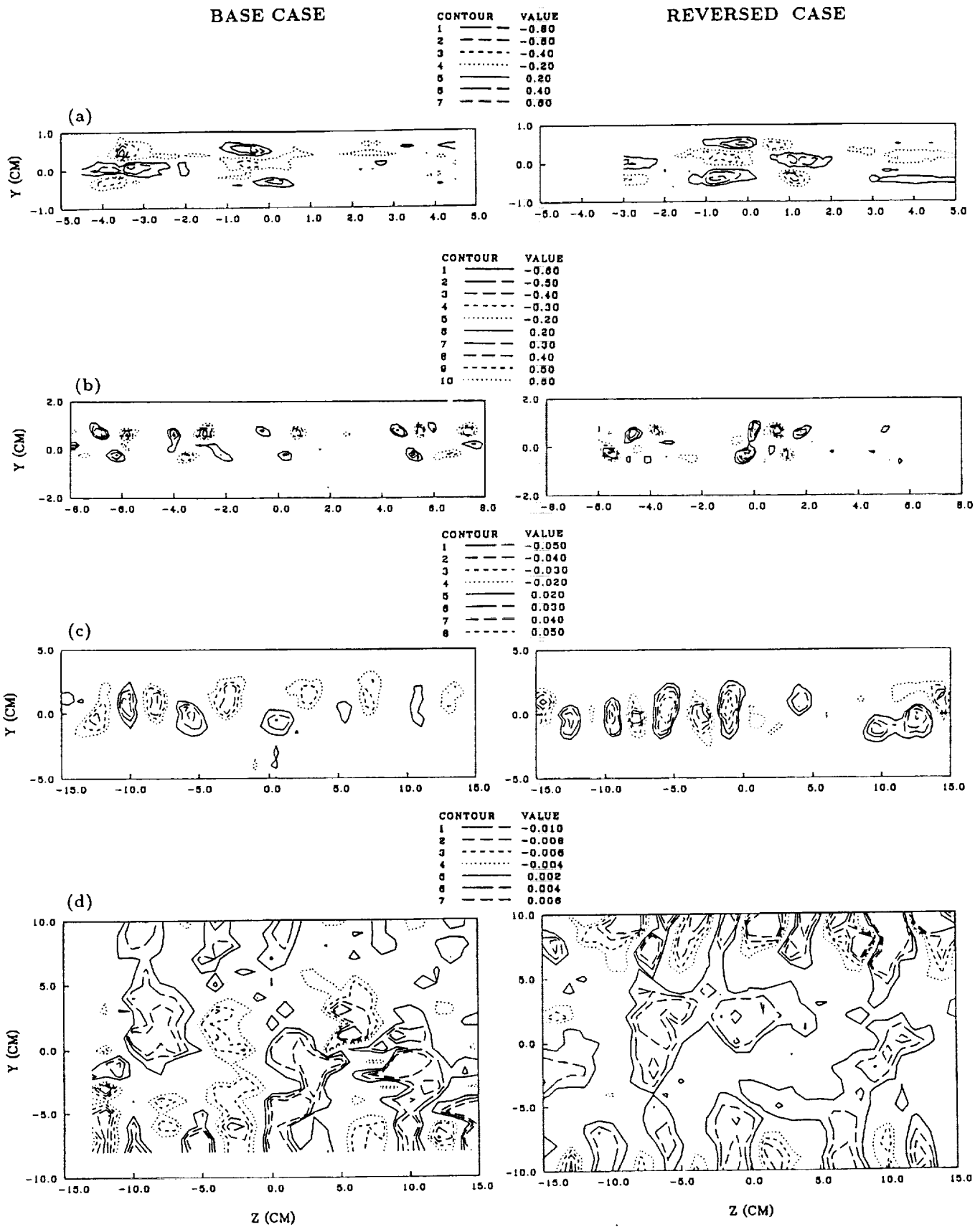

Fig. 8. Comparison of Mean Streamwise Vorticity Contours ($\Omega_x/U_0, cm^{-1}$) for Base and Reversed Cases. (a) $X = 8$ cm, (b) $X = 17$ cm, (c) $X = 77$ cm, (d) $X = 189$ cm.

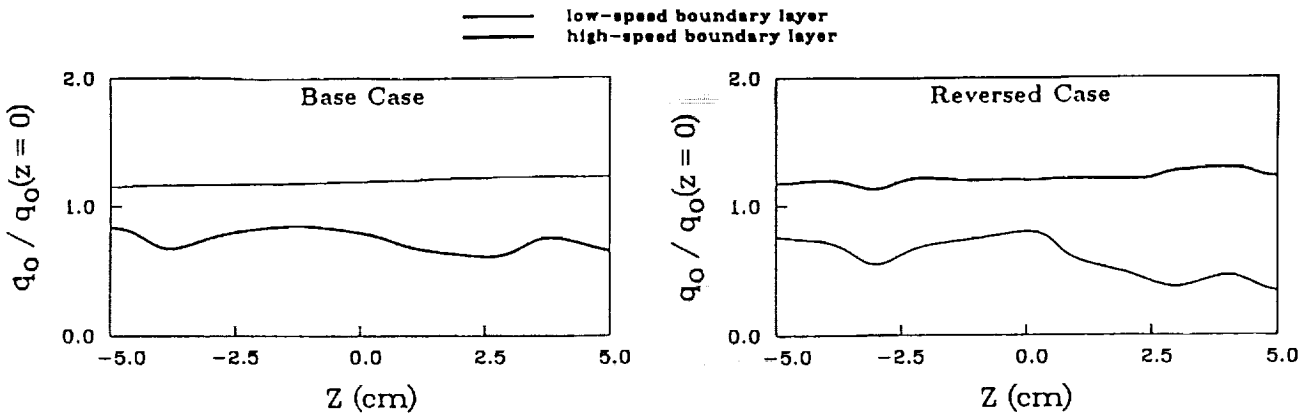

Fig. 9. Comparison of Spanwise Variation in Surface Dynamic Pressures for Base and Reversed Cases.

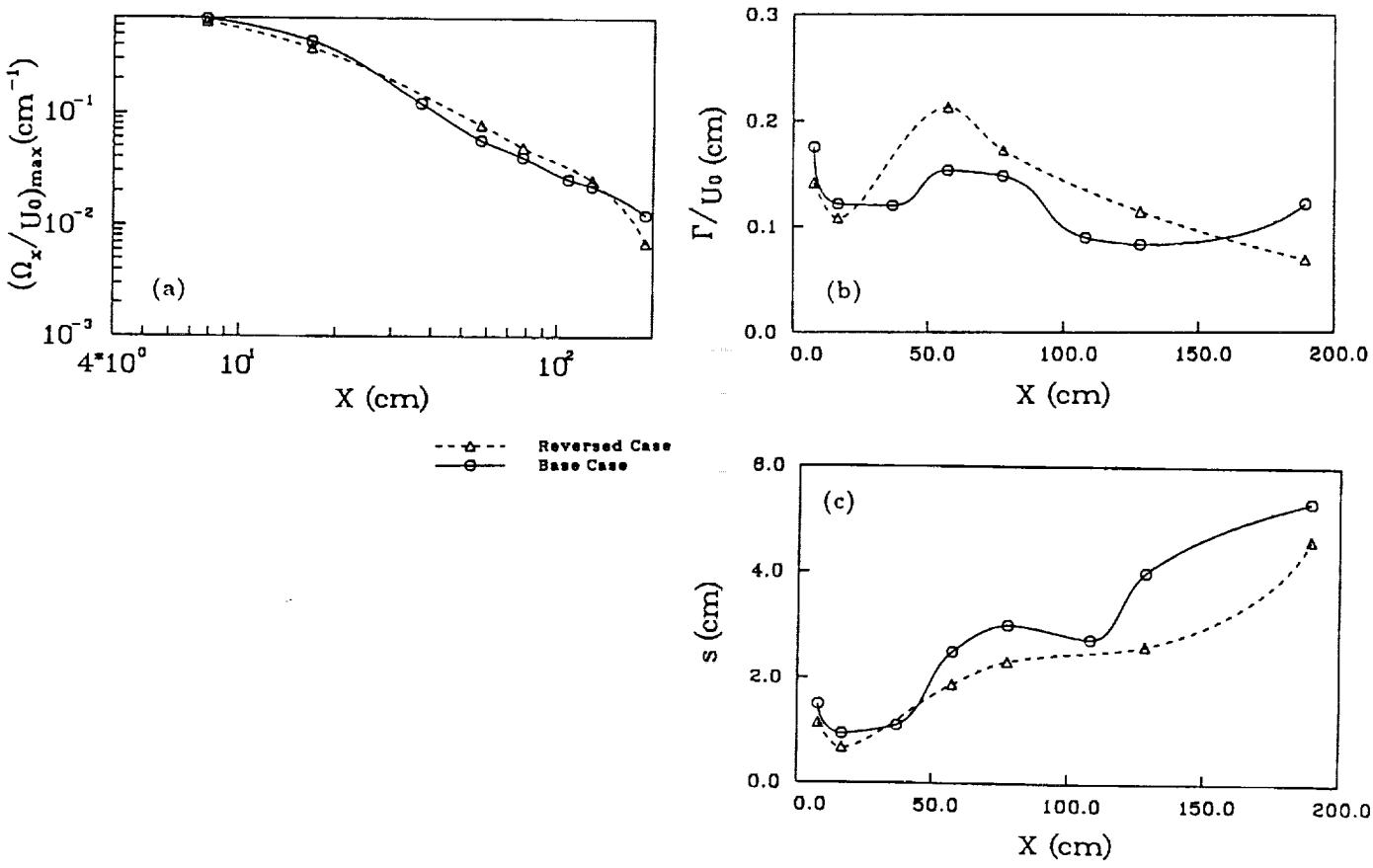

Fig. 10. Comparison of Global Streamwise Vortex Properties for Base and Reversed Cases. (a) Peak Mean Vorticity, (b) Average Vortex Circulation, (c) Vortex Spacing.